Soil Dynamics and Earthquake Engineering 99 (2017) 9–19

Contents lists available at ScienceDirect

Soil Dynamics and Earthquake Engineering

journal homepage: www.elsevier.com/locate/soildyn

Seismic response of concrete-rockfill combination dam using large-scale shaking table tests

Jianxin Wang[a], Gui Yang[b,*], Hanlong Liu[c], Sanjay Shrawan Nimbalkar[d], Xinjun Tang[e], Yang Xiao[f,*]

[a] College of Hydraulic and Civil Engineering, Xinjiang Agricultural University, Urumqi 830052, China
[b] Key Lab of Ministry of Education for Geomechanics and Embankment Engineering, College of Civil & Transportation Engineering, Hohai University, Nanjing 210098, China
[c] School of Civil Engineering, Chongqing University, Chongqing 400450, China
[d] School of Civil & Environmental Engineering, Centre for Built Infrastructure Research (CBIR), Faculty of Engineering & Information Technology, University of Technology Sydney, City Campus, 15 Broadway, Ultimo, NSW 2007, Australia
[e] College of Hydraulic and Civil Engineering, Xinjiang Agricultural University, Urumqi 830052, China
[f] College of Civil Engineering, Chongqing University, 83 Shazheng Street, Chongqing 400045, China

ARTICLE INFO

Keywords:
Concrete-rockfill combination dam
Shaking table test
Dynamic earth pressure
Residual deformation
Failure pattern

ABSTRACT

Concrete-rockfill combination dam (CRCD), a new type of dam, is mainly composed of an upstream concrete wall and a downstream inclined rockfill body. It is not in direct contact with the bedrock foundation but a water stop, which is different from conventional concrete gravity dam. The dynamic characteristics of CRCD are not quite fully understood yet. In this paper, large-scale models of CRCD were constructed and key parameters, such as acceleration-time response, dynamic earth pressure, deformation and failure pattern of slope were monitored. Results showed that the amplification factors in the upper part (0.6 H) increased with the height. The model dam showed obvious concentration and amplification effect on the low frequency component. The total earth pressure acting on the back face of the wall varied approximately nonlinear along the wall height when the PGA exceeded 0.4*g*. In addition, the CRCD model exhibited good seismic performance with small residual deformation under earthquake. A shallow sliding mode of failure at a height of 0.8 H was measured from the base on the downstream slope. Therefore, it was prudent to undertake some aseismatic reinforcement measurements at the top 1/5 thickness zone of the slope. These model test results could provide a certain reference value for preliminary understanding and qualitative analysis of a prototype CRCD.

1. Introduction

The type and size of dam are dependent upon the geology, hydrology, topography of the site as well as the availability of the construction materials. Concrete gravity dam (CGD) and concrete-faced rockfill dam (CFRD) are two most commonly used dams, among others. Concrete gravity dam (CGD) is proportioned so that itself weight alone maintains the stability, but the temperature control and cracking are major problems [1–3]. Although, CFRD is well known for convenience in construction as well as good seismic performance, its non-uniform settlement induces cracking of the concrete slab [4–7]. In view of the limitations of the conventional CGD and CFRD, a new concrete-rockfill combination dam (CRCD) was proposed. The CRCD is mainly composed of an upstream concrete wall and a downstream inclined rockfill body to bear the water pressure together. Among them, the concrete wall not only reduces the amount of concrete compared with CGD to be the anti-seepage structure of CRCD, but also enhances strength and impermeability compared with the face slab of CFRD. Moreover, the downstream inclined rockfill body could result in potential savings of construction rockfill materials in comparison with rockfill dams.

It is well known that the CGD is directly built on the bedrock to restrict its displacement. However, this renders the dam heel more prone to induce undue tensile stresses thus severely affecting stability. Rescher [8] pointed out that installing a base joint at the dam-foundation interface can reduce the tensile stress at dam heel. This paper introduces Rescher's method of installing a base joint such that the CRCD is not in direct contact with the bedrock. The CRCD can then be constructed in the bedrock or overburden foundation (see Fig. 1) by

* Corresponding authors.
E-mail addresses: wangjianxin_wjx@163.com (J. Wang), ygheitu@163.com (G. Yang), hliuhhu@163.com (H. Liu), Sanjay.Nimbalkar@uts.edu.au (S. Shrawan Nimbalkar), tangxj59@163.com (X. Tang), hhuxyanson@163.com (Y. Xiao).

http://dx.doi.org/10.1016/j.soildyn.2017.04.015
Received 18 January 2017; Received in revised form 21 March 2017; Accepted 19 April 2017
Available online 09 May 2017

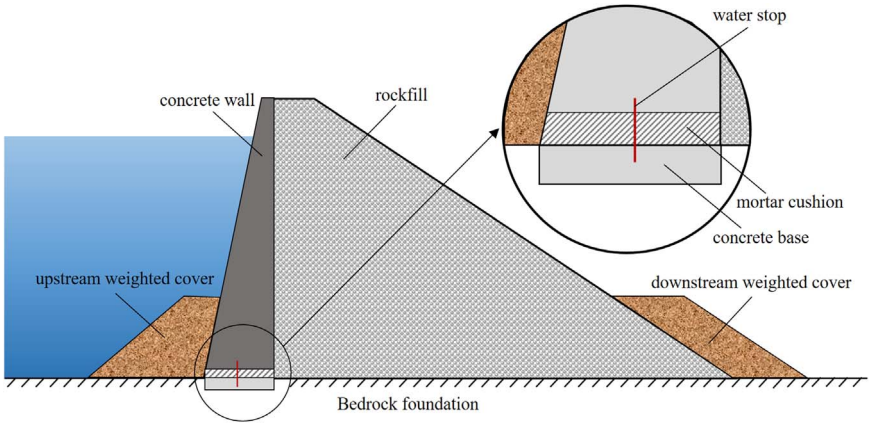

Fig. 1. Schematic diagram of CRCD.

ensuring the maximum displacement of the concrete wall base does not exceed the allowable value of the shear failure of the water stop [9–11].

Seismic analysis and evaluation of existing dams play an important role in guiding the design of new dams [12–16]. Therefore, as a new type of dam, the dynamic characteristics of CRCD need to be further studied. Shaking table test is widely used in geotechnical engineering in order to study mechanism of structure and dynamic characteristics. Centrifuge shaking table tests are generally regarded as being better than 1-g tests from the viewpoint of stress levels. However, the similitude of soil particle size is far less satisfied due to the relatively small model size. Large-scale shaking table tests are considered preferable for the present study, not only for the investigation of the seismic behaviors of dam models, but also for the validation of theoretical approaches and numerical methods commonly adopted in practice [17,18], though the scale effect is an unavoidable problem in a shaking table test.

Liu et al. [14] conducted a series of large-scale shaking table tests to investigate the dynamic failure modes of model-scale CFRD, and the findings agreed with its prototype-scale counterpart. Shi et al. [19] evaluated the dynamic deformation of landslide dams under aftershocks adopting large-scale shaking table tests. Torisu et al. [17] conducted shaking table model tests in a 1-g gravity field and hollow cylindrical torsional shear tests to verify performance-based seismic design criteria. Saleh et al. [20] studied the effect of hydrodynamic pressure on rigid and elastic dam models by conducting centrifuge shaking table tests in a N-G gravity field. Yang et al. [21] used large-scale shaking table to compare the seismic earth pressure distribution of

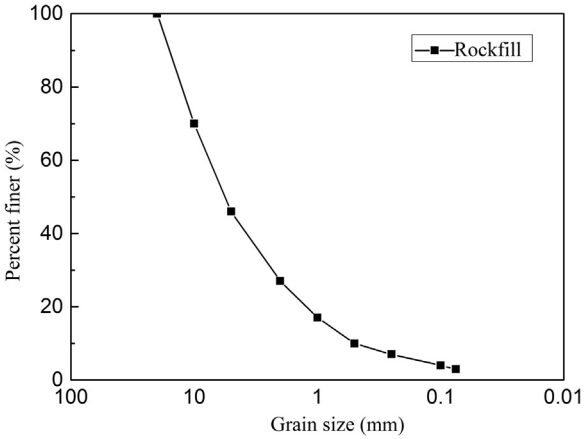

Fig. 2. Gradation curve of model materials.

Table 2
Technical parameters of the test materials.

Materials	E (GPa)	ν	ρ (g/cm^3)	c (kPa)	φ (deg)
Concrete wall	24.0	0.20	2.40	—	—
Bedrock foundation	30.0	0.25	2.40	—	—
Rockfill	0.1	0.33	1.84	40	50

Table 1
Similitude requirements.

Type	Quantity	Relationship	Similarity coefficient (prototype:model)	Prototype parameter (no prototype)	Required model parameter	Actual model parameter
Geometry property	Length (l)	C_l	30.00	30 m	1.0 m	1.0 m
Material property	Density of the rockfill (ρ)	$C_\rho = 1$	1.00	2.1g/cm^3	2.1g/cm^3	1.84g/cm^3
	Density of the concrete (ρ_c)	$C_{\rho c} = 1$	1.00	2.40g/cm^3	2.40g/cm^3	2.40g/cm^3
	Density of the water (ρ_f)	$C_{\rho f} = C_\rho$	1.00	1.00g/cm^3	1.00g/cm^3	1.00g/cm^3
	Frictional angle of rockfill (φ)	$C_\varphi = 1$	1.00	—	—	—
	Young's modulus of concrete wall (E)	$C_E = C_\rho C_l$	30	24 GPa	0.8 GPa	24 GPa
Dynamic property	Acceleration (a)	$C_a = 1$	1.00	—	—	—
	Time (t)	$C_t = C_l^{1/2}$	5.48	—	—	—
	Frequency (f)	$C_f = C_l^{-1/2}$	0.18	—	—	—

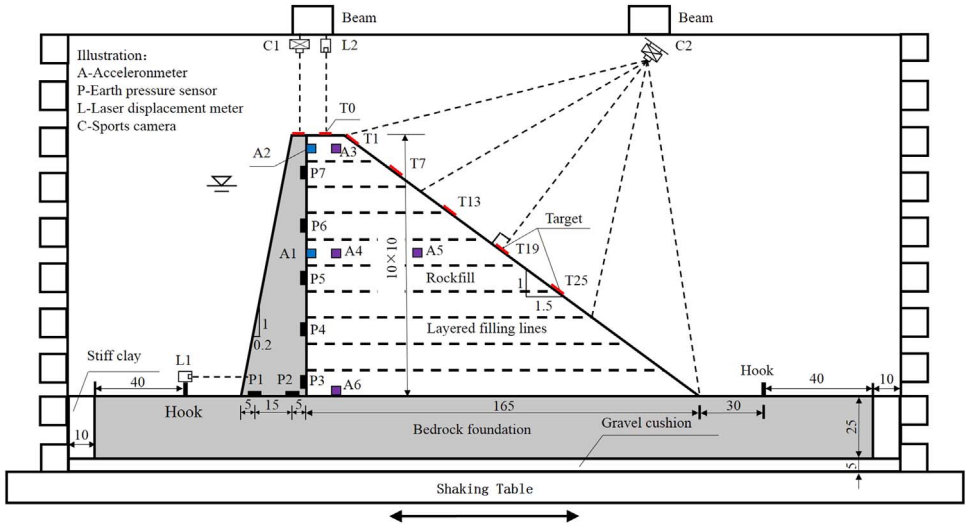

Fig. 3. Layout of CRCD model (Unit: cm).

retaining walls with different foundations. In this paper, the dynamic characteristics of CRCD are studied by large-scale shaking table. It aims to experimentally analyze the seismic response of CRCD, including the acceleration-time response, dynamic earth pressure, the deformation and the slope failure pattern.

2. Large-scale shaking table test

2.1. Model preparation

The tests were carried out at the Disaster Prevention and Mitigation Laboratory of Nanjing University of Technology. This laboratory was equipped with the earthquake simulation shaking table that was served by an electro-hydraulic energy control system. The platform size of the shaking table is 3.36 m × 4.86 m. The maximum load capacity is 25 t. The maximum horizontal driving displacement and speed are ± 120 mm and ± 500 mm/s. The maximum horizontal acceleration ($(a_h)_{max}$) is ± 1.0*g* and the working frequency (f) ranges from 0.1 to 50 Hz. The dimensions of the model box are 3.5 m (L) × 2.0 m (W) × 1.7 m (H). The model box is made of steel frame with steel plate on the bottom.

The CRCD has no practical engineering applications as a new type of dam at present. In order to investigate the dynamic characteristics of CRCD, the test was carried out with a reference height of 30 m considering the maximum working frequency of the shaking table (50 Hz). It is difficult to satisfy a complete similitude criteria in a 1-g model in shaking table test. Table 1 lists the similitude requirements, e.g., the quantities of the geometry size, the density and the acceleration as basic variables, according to Liu et al. [14]. The small-scale CRCD model tests were conducted by large-scale shaking table, the acceleration response, dynamic earth pressure, the deformation and the slope failure pattern were monitored. The model is constructed using the materials identical to the prototype. According to laboratory tests, the breakage mechanics [22] and modelling of the rockfill materials [23,24] were investigated. The stress-strain relationship of the rockfill under low and high stress magnitudes has some resemblance at the small strain level before failure [25]. It is the drawbacks in the current test that the young's modulus of concrete wall in the model CRCD is the same as that in the prototype CRCD. In addition, the interaction among the concrete wall, rockfill and dam foundation are not reflected according to the similitude law, which would be tough to deal with in a model test. Nevertheless, the model test results could provide a certain reference value for preliminary understanding and qualitative analysis for a prototype CRCD.

The gradation of the rockfill material (see Fig. 2) was determined by following the approach suggested by Varadarajan and Sharma [26]. The maximum particle size (D_{max}) of rockfill material is selected for 20 mm, the nonuniformity coefficient (C_u) is 15.0 and the curvature coefficient (C_c) is 1.5. In order to achieve desired compaction, rockfill material was divided into 10 layers, each of 100 mm in height. The weight of each layer is calculated by the controlled density. Each layer was then compacted to meet the design requirements of the placement density. The detailed parameters of the test materials used in current laboratory investigations are shown in Table 2.

The height of the CRCD model is 1 m. The upstream slope of the concrete wall is 1:0.2 and downstream slope of rockfill is 1:1.5. The width of the top of the concrete wall and rockfill downstream is 50 mm and 150 mm respectively. Some simplifications owing to limited size of the laboratory model were inevitable such as lack of (i) upstream/downstream weighted cover and (ii) water stop. The upstream of the model dam is subjected to water head of 800 mm. The model box is

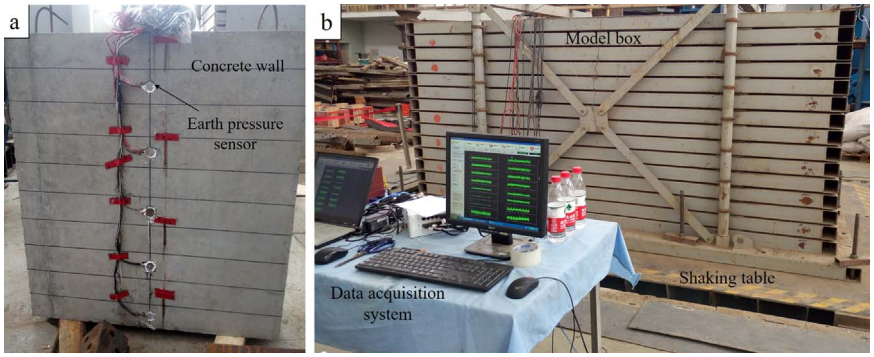

Fig. 4. Photographs of test model and data acquisition system.

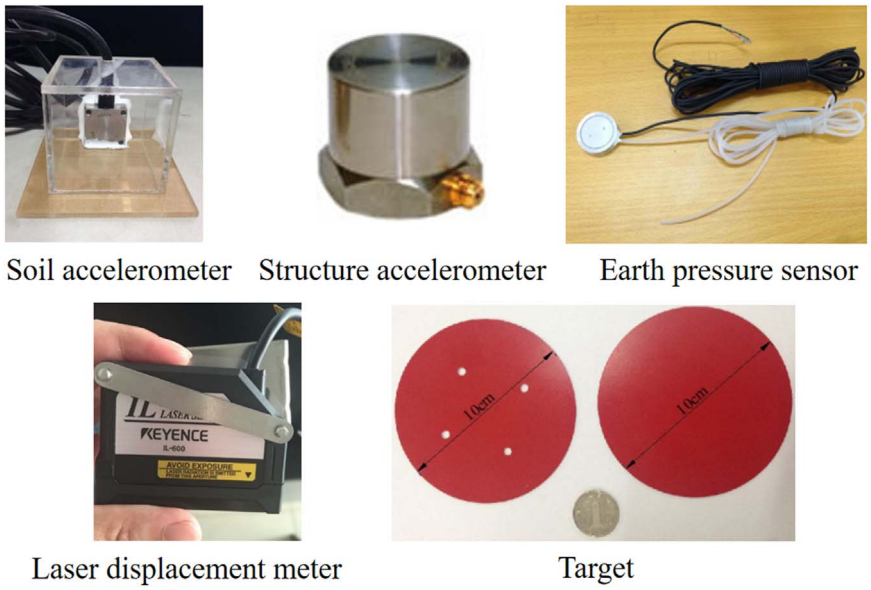

Fig. 5. Monitoring sensors of test.

bounded by 2 mm thick rubber membrane to prevent water leakage. In order to reduce the reflection of seismic waves at the boundary [27], a 50 mm thick polystyrene foam board is placed between the model dam and the box. A layer of gravel of 50 mm in thickness is used to induce friction between the bottom of box and model dam to reduce the relative displacement. Several sensors were arranged, including the structural accelerometers A1–A2, the soil accelerometers A3–A6, the laser displacement meters L1–L2, the earth pressure sensors P1–P7, the image acquisition cameras C1–C2 and several targets used to monitor deformation. The middle section of CRCD model along with the layout of sensors is shown in Fig. 3. The model and the acquisition devices are shown in Fig. 4. The monitoring sensors and parameters are shown in Fig. 5 and Table 3 respectively.

2.2. Test conditions

A white noise wave (peak ground acceleration $(a_h)_{max} = 0.02g$) was added to observe the changes of the dynamic characteristics of the model before applying seismic waves. Considering seismic wave characteristics of the ground motions, one typical middle-far-field seismic Taft (TA) wave was applied in the tests [28]. The Taft wave (a fault distance of 41 km and original peak acceleration of 0.152*g* [29]) was recorded at Taft seismologic recording station during Ms7.7 Kern Country earthquake on 21 July 1952 in California, United States. The time history records of ground acceleration and Fourier spectra of TA wave are shown in Fig. 6. The ground motion conditions for shaking test models are shown in Table 4.

3. Results and discussions

3.1. Acceleration response

The acceleration signal was corrected with a baseline method to eliminate the instability of the acceleration signal resulted from the test equipment and the environment [30]. It can be seen from Fig. 6 that most of the energy of the Taft wave is concentrated in the low frequency range of less than 50 Hz. Then the corrected acceleration data was filtered to obtain the Fourier spectra using a low-pass Butterworth filter with a cut-off frequency of 50 Hz. For brevity, only some typical results are provided herein. Figs. 7 and 8 show the variation of time history records of the ground acceleration and Fourier spectrums along the height of the CRCD, including the concrete wall, the centre line and the downstream slope. The post-earthquake phenomena reveal that the pre-vibration had little influence on CRCD when the earthquake is not very strong, which is possibly attributed to high compaction (i.e. 90% of Standard Proctor) of the rockfill. Figs. 7(a) and 8(a) show that the peak acceleration amplitudes increased with the increase of the height of the model. It was found that the peak acceleration of the model increased with increasing of the PGA. As listed in Table 5, the maximum growth rate of acceleration amplitude reached 169.17% from TA-0.2*g* to TA-0.4*g*. Furthermore, the maximum acceleration occurred at the top of the concrete wall (A2) and rockfill (A3). However, the PGA at the top of the wall was 0.248*g*, smaller than that of the rockfill ($(a_h)_{max} = 0.235g$). The same results were found in other cases, the reason for the difference will be discussed below in

Table 3
The parameters of sensors.

The test sensors	Sensor version	Main Parameters
Accelerometer	LC0108 (Soil accelerometer)	Range ± 5*g*, frequency response range 0–500 Hz, sensitivity 400 mV/g
	CA-DR-1005 M (Structure accelerometer)	Range ± 10*g*, frequency response range 0.35–4000 Hz, sensitivity 500 mV/g
Earth pressure sensor	BW	Range 100 kPa, full bridge connection, accuracy error ≤0.3 (F S)
Laser displacement meter	IL-600	Measuring distance 200–1000 mm, linearity ± 0.25%, IP67 protection grade, red semiconductor laser, visible light wavelength 655 nm

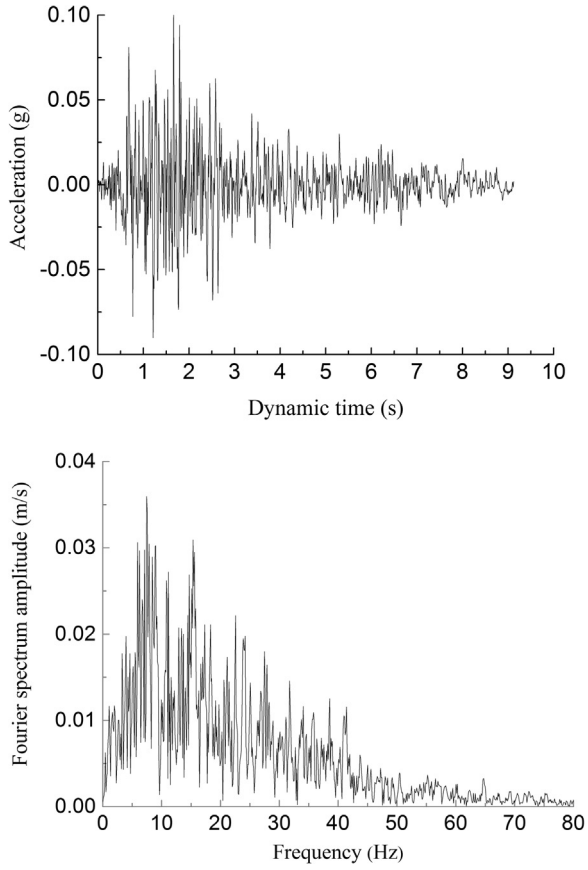

Fig. 6. Input time history records of earthquake acceleration and Fourier spectra.

Table 4
Loading cases for shaking table test.

Test numbers	Input excitation	Test case	Duration (s)	PGA (g)	Water depth (m)
1	White noise	WN-0.02*g*	180.00	0.02	0.00
2	Taft wave	TA-0.1*g*-W	9.12	0.10	0.80
3	Taft wave	TA-0.2*g*-W	9.12	0.20	0.80
4	Taft wave	TA-0.4*g*-W	9.12	0.40	0.80
5	Taft wave	TA-0.6*g*-W	9.12	0.60	0.80

detail.

As shown in Figs. 7(b) and 8(b), the spectrum characteristics obviously changed at different positions of the model and different ground motions, particularly along the centre line of rockfill portion of CRCD. The Fourier spectra occurred double peaks in TA-0.1*g*. Their predominant frequencies were concentrated at three peak points of 8.90 Hz, 27.60 Hz and 31.88 Hz, respectively. The spectral characteristics changed from the bottom to the top of the model with the increase in the input peak acceleration. High frequency components of the ground motion gradually reduced while low frequency components increased. The Fourier spectrum changed from double peaks to single one from Test 2 to Test 5. The frequency was concentrated at 7.50 Hz under the condition of TA-0.6*g*. The results exhibited obvious concentration and amplification effect on the low frequency component [31]. The high frequency components of seismic waves were gradually filtered while the low ones were enlarged with the increase of PGA. The results could be attributed to the reduction of stiffness and the increase in damping of the rockfill materials.

The difference of Fourier spectrum between concrete wall and rockfill is very small. Thus, the Fourier spectra of dam crest (rockfill) under different ground motions were plotted in Fig. 9. The Fourier spectrum changed from double peaks to single one with the increase of the PGA. Its maximum frequency was concentrated at 7.50 Hz (see Fig. 9(a)). As shown in Fig. 9(b), the predominant frequency for CRCD ranged from 5.4 to 9.2 Hz [32]. The closer the predominant frequency of the input seismic wave gets to the fundamental frequency (the average frequency of 10.1 Hz measured in Test 1), the greater the seismic response becomes.

Acceleration amplification factor is ratio of PGA to the maximum acceleration measured [18]. Distribution of the acceleration amplification factor of the concrete wall is shown in Fig. 10. It shows the variation of acceleration amplification factor along the height of concrete wall. It is seen that the acceleration increased with the height [28]. Results show that the acceleration amplification factor can increase up to 2.67 at the top of the wall ($H = 0.95$ m). This finding also reveals that the acceleration amplification effect is obvious at the top of the concrete wall.

Fig. 11 shows the distribution of peak acceleration and the amplification factor along the height of the rockfill. Combined with Table 5 above, it was found that the peak acceleration of the rockfill increased with the increase of the amplitude of the seismic waves, and the acceleration response at the top of the rockfill was the greatest [32]. The peak acceleration increased significantly from 0.4*g* and it could reach the maximum value of 1.13*g*. The acceleration amplification factor of the rockfill decreased with the increase of the peak acceleration [14,18,20]. The amplification factors in the lower part of the dam does not change much, however, the amplification factors in the upper part (0.6 H) show large increase with the height. When the maximum bedrock acceleration of 0.4*g* was excited, the amplification factor between the base and the crest increased significantly to almost 2.48. On the other hand, the resistance against the movement of the rockfill particles decreased leading to that a significant acceleration amplification effect in the top of model dam when the CRCD model was subjected to strong earthquake [33]. The waterproofing rubber membrane and gravel cushion at the bottom of the model box could result into acceleration amplification factor of A6 to be less than 1.0 in some cases.

Table 6 shows the comparison of acceleration amplification factor at the top of the concrete wall and rockfill. According to the test results reported earlier, the effect of the acceleration amplification is the most obvious for both at the top of the concrete wall and rockfill. Therefore, only the seismic response at the top position is selected for comparison in the section. It is evident from the table that acceleration amplification factor at the top of the wall (A2) is greater than that of the rockfill (A3). This is because the low stiffness of the rockfill compared with the concrete wall. In addition, the damping of rockfill increases with the progress of the earthquake action, which consumes more energy as the seismic waves propagate upward to the crest.

3.2. Dynamic earth pressure

In order to avoid the superposition effect of the test results, the previous dynamic pressure monitored will be reset before next test condition starts. The earth pressure sensors only recorded the increment of the earth pressure caused by different seismic waves, rather than the continuous process of whole duration of the earthquake. Fig. 12 presents the dynamic earth pressure records at the bottom of the wall under the condition of TA-0.4*g*-W. The peak dynamic earth pressure at

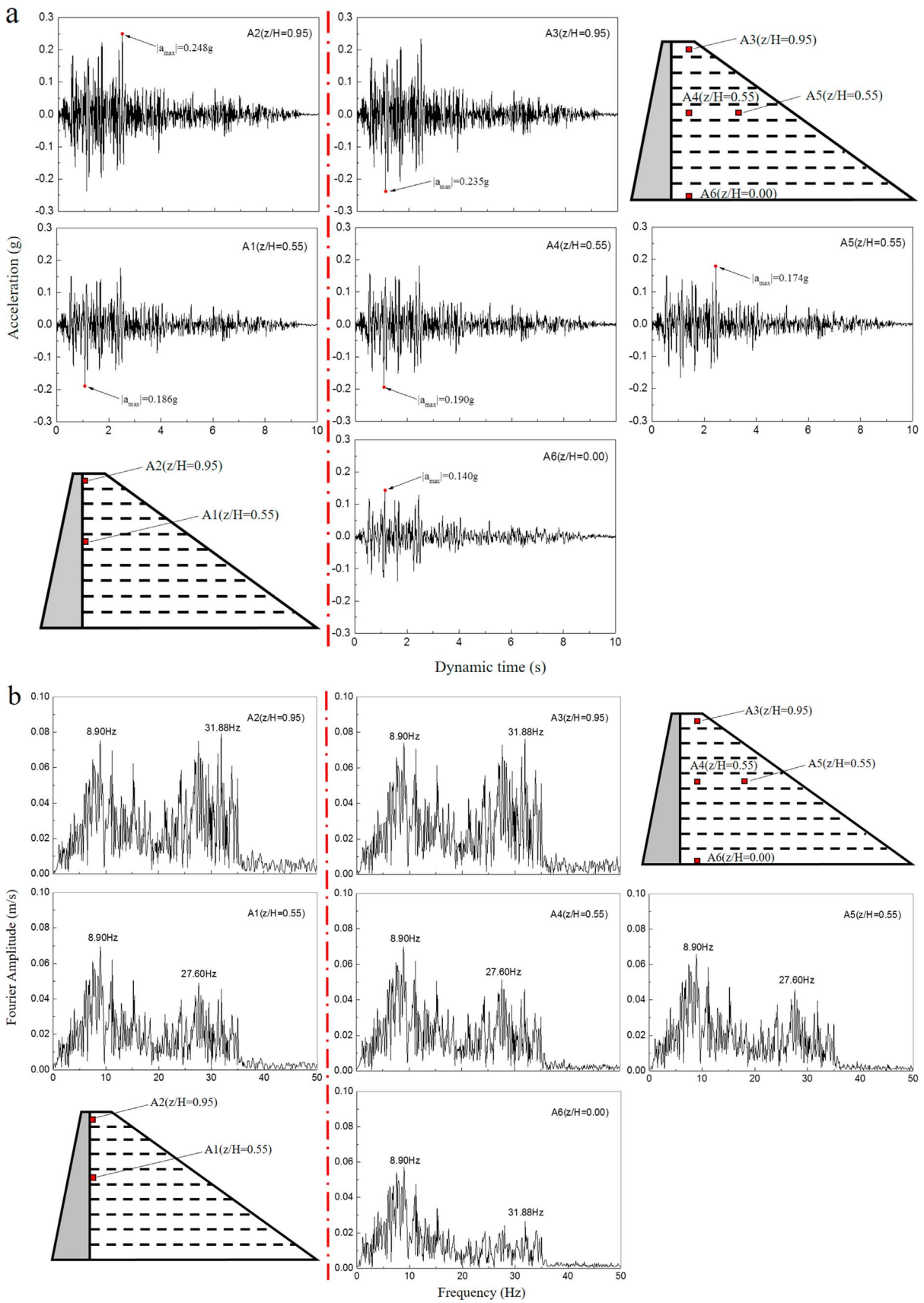

Fig. 7. Records of acceleration-time history and Fourier spectra at different height of the CRCD model (Test 2, maximum bedrock acceleration = 0.1*g*).

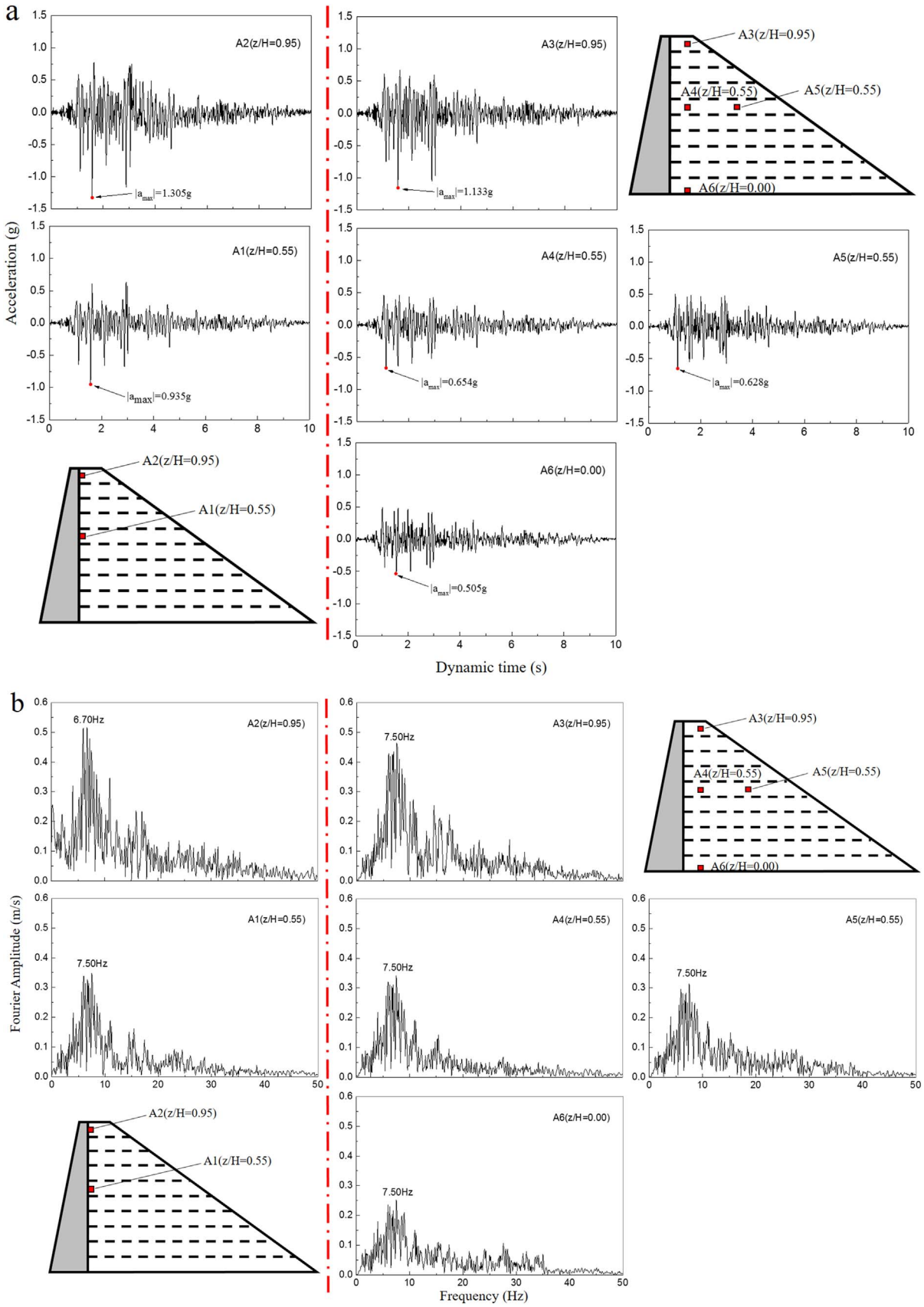

Fig. 8. Records of acceleration-time history and Fourier spectra at different height of the CRCD model (Test 5, maximum bedrock acceleration = 0.6*g*).

Table 5
Comparison of acceleration amplitude and growth rate.

Position	TA-0.1g-W		TA-0.2g-W		TA-0.4g-W		TA-0.6g-W
	Amplitude(g)	Growth rate	Amplitude(g)	Growth rate	Amplitude(g)	Growth rate	Amplitude(g)
A1	0.186	39.10%	0.259	148.34%	0.644	45.24%	0.935
A2	0.248	60.08%	0.397	169.17%	1.069	22.09%	1.305
A3	0.235	62.66%	0.382	159.23%	0.991	14.32%	1.133
A4	0.190	42.21%	0.270	83.59%	0.496	31.83%	0.654
A5	0.174	48.01%	0.258	80.09%	0.464	35.30%	0.628
A6	0.140	56.59%	0.220	76.95%	0.388	30.11%	0.505

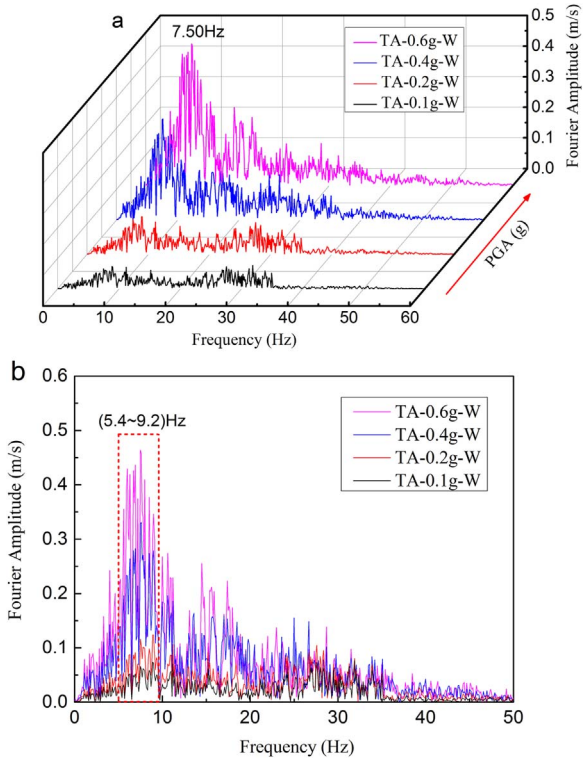

Fig. 9. Fourier spectra of dam crest under different ground motions.

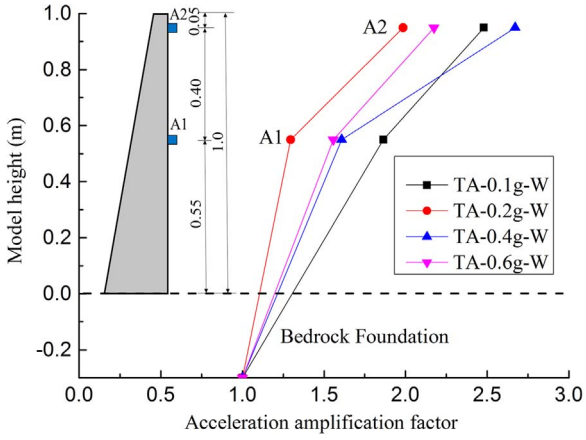

Fig. 10. The distribution of acceleration amplification factor along the height of concrete wall.

the toe ($P1_{max}$) and heel ($P2_{max}$) are 1.80 kPa and 8.76 kPa, respectively. Fig. 13 shows that the dynamic earth pressure at the bottom of the wall was positive during the earthquake. The dynamic earth pressure at the bottom of the wall increased with the increase of the peak acceleration, in agreement with findings reported elsewhere [34]. The direction of bending moment of concrete wall pointed to the downstream under the action of ground motion and hydrodynamic pressure. Since the centre of gravity of the wall was also biased downstream, the dynamic earth pressure at the toe (P1) was less than that of heel P2. The results showed that the wall turns to the downstream direction under the water storage conditions.

The total earth pressure is obtained by the combination of dynamic earth pressure and static earth pressure and is shown in Fig. 14. The total dynamic earth pressure acting on the back face of the wall increases with the increase of the peak acceleration basically [21,35]. The total earth pressure showed approximate linear distribution along the wall height under the condition of PGA of 0.1*g* and 0.2*g*. The total earth pressure showed a significant nonlinear variation for PGA larger than 0.4*g*. The total earth pressure of at the bottom of the wall was found to be the greatest, while the small value obtained near the top. Results also indicated that the dynamic displacements were largest at the top of the wall. The displacement leads to the less contact with the rockfill at the top resulting in a smaller total earth pressure [35,36]. With closer contact with the downstream rockfill, the bottom of the wall showed a larger value of total earth pressure. The value of the total earth pressure increment between P3 and P7 at the back of the wall (ΔP) and the cumulative displacement at the bottom of the wall (S) are plotted in Fig. 15. Result shows that the total incremental dynamic earth pressure of the wall back not only increased with the increase of the peak acceleration but also varied linearly with the cumulative displacement at the bottom of the wall.

3.3. Residual deformation

Fig. 16 shows the settlement at the top of the rockfill. It is shown that the vertical displacement of the dam crest increased with the vibration time of the seismic wave input. The maximum residual settlement was 1.016 mm, which was found at 4.21 s, showing significant time lag compared to the occurrence of peak acceleration. This is attributed to the lagging of rockfill material [16,37]. Table 7 shows the residual horizontal and vertical displacements measured at the wall top and the residual horizontal displacement measured at the top of the rockfill. The residual horizontal displacement at the bottom of the concrete wall was found to only 0.567 mm, 0.06% of the wall height, and it did not exceed the allowable value of the shear failure of the water stop [9]. The residual horizontal displacement of the top of the wall was 1.243 mm, 0.12% of the height. Furthermore, the horizontal displacement at the top of the wall was greater than that of the bottom. As evident from Table 7, it could be seen that the concrete wall turned to the direction of rockfill around the bottom of the wall. The residual displacement of the top of the rockfill was 0.52 mm, accounting for 0.05% of the dam height. And the residual settlement of the top of the rockfill was 2.26 mm, 0.23% of the height [18]. In summary, the residual deformation of the CRCD under the earthquake is relatively small, which emphasizes good performance of CRCD under seismic environment.

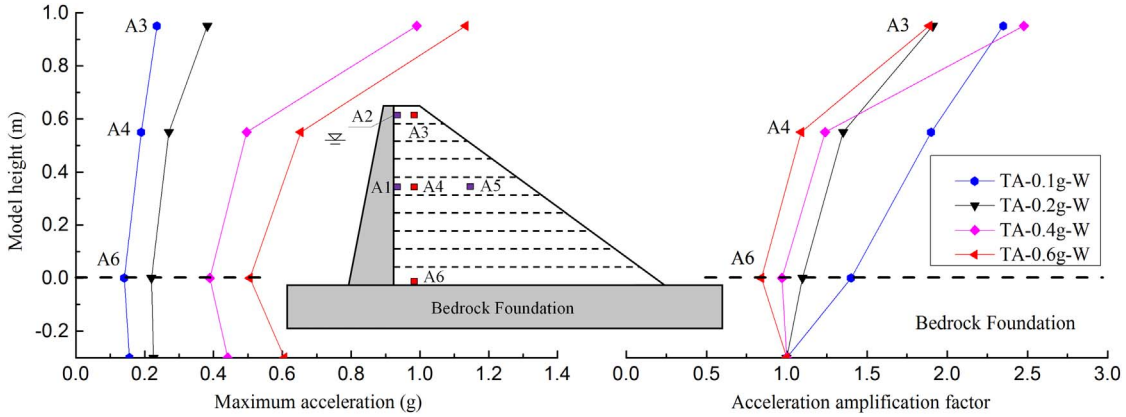

Fig. 11. Acceleration amplification factor of rockfill under different ground motions.

Table 6
Comparison of acceleration amplification factor between the concrete wall and the rockfill.

Test numbers	Test case	Acceleration amplification factors	
		A2	A3
2	TA-0.1g-W	2.48	2.35
3	TA-0.2g-W	1.98	1.91
4	TA-0.4g-W	2.67	2.48
5	TA-0.6g-W	2.17	1.89

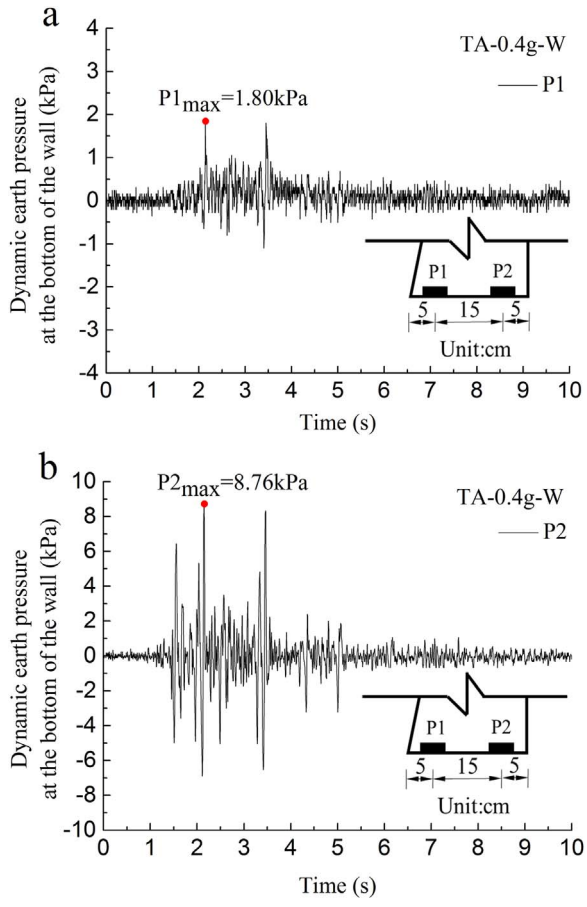

Fig. 12. Transient records of dynamic earth pressure at the bottom of the wall.

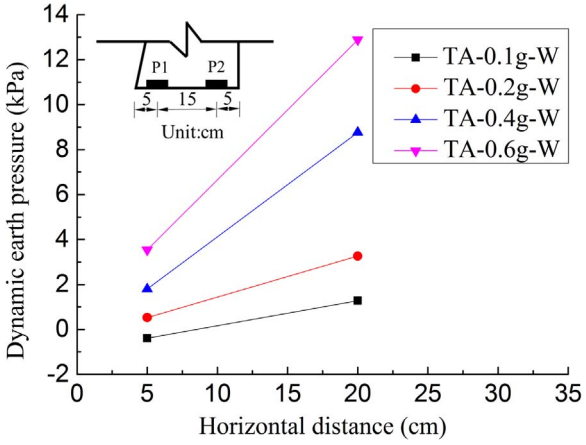

Fig. 13. The distribution of maximum dynamic earth pressure at the bottom of the concrete wall.

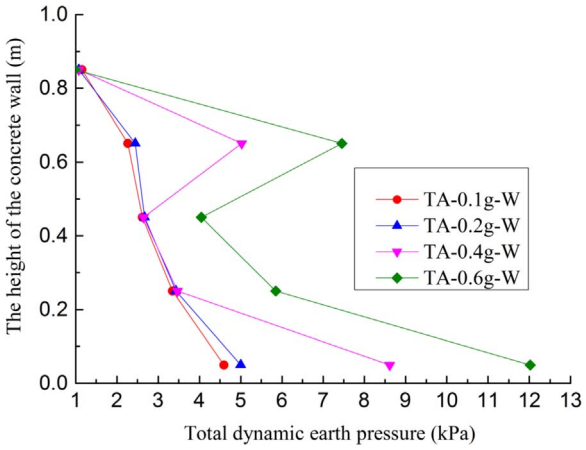

Fig. 14. Distribution of total dynamic earth pressure along the height of concrete wall.

3.4. Failure pattern

In order to investigate the slope failure pattern in CRCD, the targets were installed on the downstream slope, where they were traced by cameras during the tests (see Fig. 3). According to the imaging observations, a small number of rockfill materials felt down and slid toward the downstream direction occurring on the surface of the slope. Fig. 17 shows the displacement of targets (T1/T7/T13) along the

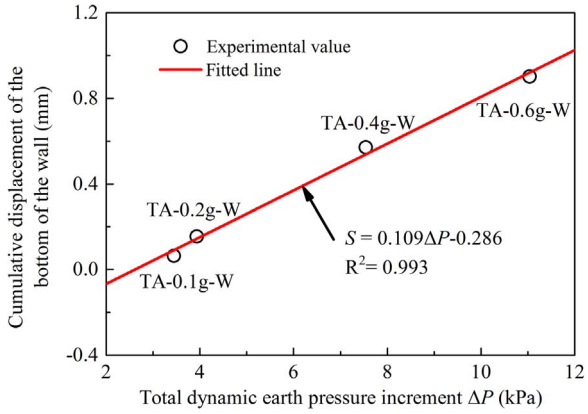

Fig. 15. Variation between total earth pressure increment and the residual displacement of the wall.

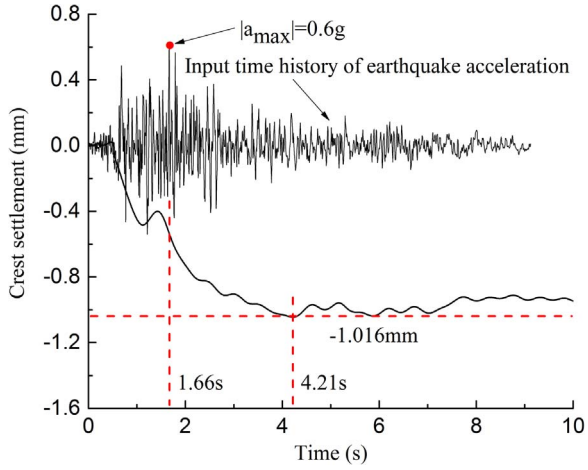

Fig. 16. Crest settlement at the top of the rockfill (TA-0.6*g*-W).

downstream direction of slope obtained by a vision-based displacement test method [29]. Displacements of the slope decreased toward the downstream direction and the maximum displacement (T1) was 1.767 mm near the dam crest. According to the test phenomenon, the failure started in the form of sliding accompanied by some rockfill particles falling down on the surface of the downstream slope near the dam crest. This was followed by a shallow block of rockfill sliding down along the downstream slope [17,38]. In summary, shallow sliding at 0.8 H on the downstream slope was found to be the main slope failure pattern observed in CRCD.

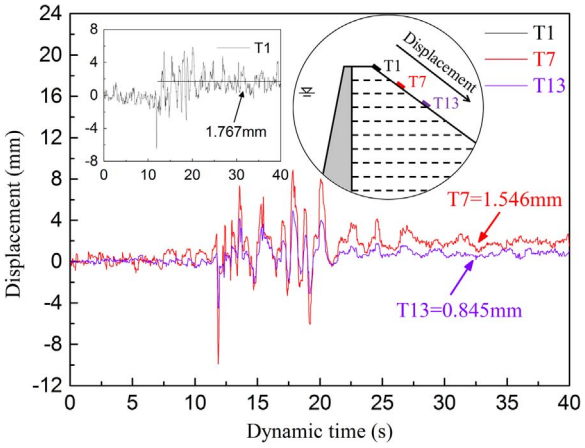

Fig. 17. Displacement along the downstream direction of slope (TA-0.6*g*-W).

4. Conclusions

Large-scale shaking table tests were conducted to study the seismic response of CRCD. The carefully designed performed shaking table tests could reproduce the key features of the responses of the large-scale models under laboratory based earthquake simulations. The sensors provided the continuous measurement of acceleration, dynamic earth pressure, the deformation and the slope failure pattern of the dam during the whole test duration. Based on the experimental findings, the following conclusions can be drawn:

(1) CRCD model had an obvious amplification effect on the input of seismic waves. The amplification factors in the upper part (0.6 H) increased greatly with the height. The high frequency components of seismic waves were gradually filtered while the low ones were enlarged with the increase of PGA. The results exhibited obvious concentration and amplification effect on the low frequency component, which was possibly attributed to the stiffness reduction and damping increase in the CRCD model.

(2) The distribution of dynamic earth pressure as well as the total earth pressure both increased with the increase of the peak acceleration. The total earth pressure acting on the back face of the wall varied approximately linear along the wall height under PGA 0.1*g* and 0.2*g*. Nevertheless, it showed a significant nonlinear distribution when the PGA exceeded 0.4*g*. Furthermore, the total incremental dynamic earth pressure was not only increased with the increase of the peak acceleration, but also was found to linearly vary with the cumulative displacement at the wall base.

(3) The proportion of the residual horizontal displacement of the wall to the dam height ranged from 0.06% to 0.12%. The maximum horizontal displacement on the dam crest was 0.05% of the dam height while the residual crest settlement was only 0.23%. In

Table 7
The residual deformations observed in the laboratory CRCD model.

Test numbers	Test case	Horizontal displacement of the bottom of the wall (mm)	Horizontal displacement of the top of the wall (mm)	Horizontal displacement of the top of rockfill (mm)	Crest settlement of rockfill (mm)
2	TA-0.1*g*-W	0.082	0.105	0.094	−0.119
3	TA-0.2*g*-W	0.087	0.183	0.055	−0.111
4	TA-0.4*g*-W	0.143	0.325	0.104	−1.010
5	TA-0.6*g*-W	0.254	0.630	0.267	−1.016
Total residual deformation (mm)		0.567	1.243	0.520	−2.256
Proportion of the total residual deformation to the dam height		0.06%	0.12%	0.05%	0.23%

summary, the residual deformation of the CRCD under the earthquake was relatively small, indicating a good seismic performance.

(4) According to the investigation of the slope failure pattern of CRCD, displacements of the slope decreased toward the downstream direction and the maximum displacement was near the dam crest. The slope failure pattern of CRCD mainly was in the form of shallow sliding occurring at the height of 0.8 H on the downstream slope. To ensure slope stability, some aseismatic reinforcement measures should be taken at the top 0.2 H zone of the slope.

Acknowledgments

The authors would like to acknowledge the financial support from the 111 Project of China (Grant no. B13024) and the National Natural Science Foundation of China (Grant nos. 51479059 and 51509024).

References

[1] Bazant ZP. Is no-tension design of concrete or rock structures always safe? – fracture analysis. J Struct Eng 1996;122(1):2–10.
[2] Bouzoubaâ N, Lachemi M, Miao B, Aïtcin PC. Thermal damage of mass concrete: experimental and numerical studies on the effect of external temperature variations. Can J Civil Eng 1997;24(4):649–57.
[3] Campos A, López C, Blanco A, Aguado A. Structural diagnosis of a concrete dam with cracking and high nonrecoverable displacements. J Perform Constr Fac 2016;30(5):04016021.
[4] Xu B, Zou DG, Liu HB. Three-dimensional simulation of the construction process of the Zipingpu concrete face rockfill dam based on a generalized plasticity model. Comput Geotech 2012;43(6):143–54.
[5] Zhang G, Zhang JM. Modeling of low-cement extruded curb of concrete-faced rockfill dam. Can Geotech J 2011;48(1):89–97.
[6] Bayraktar A, Kartal ME, Adanur S. The effect of concrete slab–rockfill interface behavior on the earthquake performance of a CFR dam. Int J Nonlinear Mech 2011;46(1):35–46.
[7] Arici Y. Evaluation of the performance of the face slab of a CFRD during earthquake excitation. Soil Dyn Earthq Eng 2013;55(6):71–82.
[8] Rescher OJ. Arch dams with an upstream base joint. Int Water Power Dam Constr 1993;45(3):17–25.
[9] USACE. Waterstops and other preformed joint materials for civil works structures EM 1110-2-2102. US Army Corps of Engineers, Washington, DC; 1995.
[10] Zhang CH, Xu YJ, Wang GL, Jin F. Non-linear seismic response of arch dams with contraction joint opening and joint reinforcements. Earthq Eng Struct D 2000;29(10):1547–66.
[11] Haririardebili MA, Kianoush MR. Seismic analysis of a coupled dam-reservoir-foundation system considering pressure effects at opened joints. Struct Infrastruct E 2015;11(7):833–50.
[12] Wang GH, Wang YX, Zhou W, Zhou CB. Integrated duration effects on seismic performance of concrete gravity dams using linear and nonlinear evaluation methods. Soil Dyn Earthq Eng 2015;79:223–36.
[13] Liu HL, Chen YM, Yu T, Yang G. Seismic analysis of the Zipingpu concrete-faced rockfill dam response to the 2008 Wenchuan, China, Earthquake. J Perform Constr Fac 2013;29(5):04014129.
[14] Liu J, Liu FH, Kong XJ, Yu L. Large-scale shaking table model tests on seismically induced failure of concrete-faced rockfill dams. Soil Dyn Earthq Eng 2016;82:11–23.
[15] Leger P, Javanmardi F. Seismic stability of concrete gravity dams strengthened by rockfill buttressing. Soil Dyn Earthq Eng 2007;27(3):274–90.
[16] Noorzad R, Omidvar M. Seismic displacement analysis of embankment dams with reinforced cohesive shell. Soil Dyn Earthq Eng 2010;30(11):1149–57.
[17] Torisu SS, Sato J, Towhata I, Honda T. 1-G model tests and hollow cylindrical torsional shear experiments on seismic residual displacements of fill dams from the viewpoint of seismic performance-based design. Soil Dyn Earthq Eng 2010;30(6):423–37.
[18] Yuan LJ, Liu XS, Wang XG, Yang YS, Yang ZQ. Seismic performance of earth-core and concrete-faced rock-fill dams by large-scale shaking table tests. Soil Dyn Earthq Eng 2014;56(1):1–12.
[19] Shi ZM, Wang YQ, Peng M, Guan SG, Chen JF. Landslide dam deformation analysis under aftershocks using large-scale shaking table tests measured by videogrammetric technique. Eng Geol 2015;186:68–78.
[20] Saleh S, Madabhushi S. Hydrodynamic pressures behind flexible and rigid dams. Dams Reserv 2010;20(2):73–82.
[21] Yang CW, Zhang JJ, Qu HL, Bi JW, Liu FC. Seismic earth pressures of retaining wall from large shaking table tests. Adv Mater Sci Eng 2015:1–8.
[22] Xiao Y, Liu HL. Elastoplastic constitutive model for rockfill materials considering particle breakage. Int J Geomech 2016;17(1):04016041. http://dx.doi.org/10.1061/(ASCE)GM.1943-5622.0000681.
[23] Xiao Y, Liu HL, Desai CS, Sun YF, Liu H. Effect of intermediate principal-stress ratio on particle breakage of rockfill material. J Geotech Geoenviron 2016;142(4):06015017. http://dx.doi.org/10.1061/(ASCE)gt.1943-5606.0001433.
[24] Xiao Y, Liu H, Chen Y, Jiang J. Bounding surface model for rockfill materials dependent on density and pressure under triaxial stress conditions. J Eng Mech 2014;140(4):04014002. http://dx.doi.org/10.1061/(ASCE)EM.1943-7889.0000802.
[25] Xiao Y, Liu H, Chen Y, Jiang J. Strength and deformation of rockfill material based on large-scale triaxial compression tests. I: influences of density and pressure. J Geotech Geoenviron 2014;140(12):04014070. http://dx.doi.org/10.1061/(ASCE)GT.1943-5606.0001176.
[26] Varadarajan A, Sharma KG, Abbas SM, Dhawan AK. Constitutive model for rockfill materials and determination of material constants. Int J Geomech 2006;6(4):226–37.
[27] Srilatha N, Latha GM, Puttappa CG. Effect of frequency on seismic response of reinforced soil slopes in shaking table tests. Geotext Geomembr 2013;36(1):27–32.
[28] Wang LY, Chen GX, Chen S. Experimental study on seismic response of geogrid reinforced rigid retaining walls with saturated backfill sand. Geotext Geomembr 2015;43(1):35–45.
[29] Chen GX, Chen S, Qi CZ, Du XL, Wang ZH, Chen WY. Shaking table tests on a three-arch type subway station structure in a liquefiable soil. B Earthq Eng 2015;13(6):1675–701.
[30] Yang J, Li J, Lin G. A simple approach to integration of acceleration data for dynamic soil–structure interaction analysis. Soil Dyn Earthq Eng 2006;26(8):725–34.
[31] Chen GX, Wang ZH, Zuo X, Du XL, Gao HM. Shaking table test on the seismic failure characteristics of a subway station structure on liquefiable ground. Earthq Eng Struct D 2013;42(10):1489–507.
[32] Kim MK, Lee SH, Choo YW, Kim D-S. Seismic behaviors of earth-core and concrete-faced rock-fill dams by dynamic centrifuge tests. Soil Dyn Earthq Eng 2011;31(11):1579–93.
[33] Yang G, Yu T, Yang X, Han B. Seismic resistant effects of composite reinforcement on rockfill dams based on shaking table tests. J Earthq Eng 2016:1–13.
[34] Wang YZ. Distribution of earth pressure on a retaining wall. Geotechnique 2000;50(1):83–8.
[35] Ishibashi I, Fang YS. Dynamic earth pressures with different wall movement modes. Soils Found 1987;27(4):11–22.
[36] Nishimura S, Takahashi H, Morikawa Y. Observations of dynamic and non-dynamic interactions between a quay wall and partially stabilised backfill. Soils Found 2012;52(1):81–98.
[37] Albano M, Modoni G, Croce P, Russo G. Assessment of the seismic performance of a bituminous faced rockfill dam. Soil Dyn Earthq Eng 2015;75:183–98.
[38] Liu J, Liu FH, Kong XJ, Yu L. Large-scale shaking table model tests of aseismic measures for concrete faced rock-fill dams. Soil Dyn Earthq Eng 2014;61:152–63.